Combined microfluidics/protein patterning platform for pharmacological interrogation of axon pathfinding†

Peng Shi,[a] Stephane Nedelec,[b] Hynek Wichterle[b] and Lance C. Kam*[a]

Received 23rd October 2009, Accepted 5th January 2010
First published as an Advance Article on the web 25th January 2010
DOI: 10.1039/b922143c

Assembly of functional neural circuits relies on the ability of axons to navigate a complex landscape of guidance cues in the extracellular environment. In this report, we investigate localized cell signaling in response to these cues by combining a microfabricated compartmentalization chamber with multicomponent, protein-micropatterned surfaces; this system offers improved spatial resolution and new capabilities for targeted manipulation of neuronal axons. We illustrate the potential of this system by addressing the role of fibroblast growth factor receptor (FGFR) signaling in modulating axon guidance by *N*-cadherin. Motor neurons that were derived from embryonic stem cells extend axons from one compartment through a microchannel barrier and into a second compartment containing patterns of *N*-cadherin, against a background of laminin. *N*-cadherin was effective in both guiding and accelerating motor axon outgrowth. Using the chamber system to target the application of pharmacological agents to specific parts of the neuron, we demonstrate that FGFR signaling in the axon but not the cell body increases the rate of axon outgrowth while not affecting guidance along *N*-cadherin. These results demonstrate that cell signaling must take into account the spatial layout of the cell. This new platform provides a powerful tool for understanding such effects over a wide range of signaling systems.

Introduction

Proper function of the nervous system relies on the formation of precise neuronal connections that traverse complex substrates and span long distances. During neural development axons navigate to their appropriate targets by responding in a cell type specific manner to multiple signals presented in the extracellular environment.[1] These cues come from a wide range of signaling systems, including "canonical" guidance molecules (*e.g.* Netrins, Slits, Semaphorins, and Ephrins), morphogens (*e.g.* Hedgehog, BMP, and Wnt families), growth factors (*e.g.* NGF, BDNF, HGF, and FGFs), and cell adhesion proteins (*e.g. N*-cadherin, NCAM, L1-CAM). Extensive crosstalk between these pathways has been demonstrated, introducing an additional layer of complexity to the mechanisms controlling axonal navigation. Most guidance molecules are associated with the extracellular matrix and are therefore received and interpreted by nerve cells in a highly localized manner within the growth cones found at the tips of growing axons. Axon guidance is thus an intricate process occurring on a subcellular scale, requiring highly refined experimental techniques to study and manipulate.

Contemporary microfabrication methods expand and enhance the set of tools to study localized signaling mechanisms. For example, Campenot chambers, which consist of millimetre-scale barriers that isolate axons and cell bodies into separate compartments, have been widely used to investigate local function of neurotrophic factors by restricting the activity of pharmacological agents to distinct parts of the neuron.[2–4] This allows localized study of receptors on the cell surface and limits the effects of detrimental or toxic drugs to the rest of the cell. Microfabricated versions of the Campenot chamber have been more recently developed that provide higher reproducibility and better compatibility with a broad range of nerve cells by eliminating the need for a sealant compound between the chamber and substrate through which neurons must extend their axons.[5–8] The classic stripe assay method, in which matrices are patterned with two different guidance molecules to study axonal substrate preference, has similarly been updated by microfabrication. Specifically, the use of microfluidics and microcontact printing methods allows patterning of finer features as well as the combination and alignment of more than two molecular cues.[9,10]

In this report, we combine the benefits of microfabricated Campenot chambers with those of protein-micropatterned surfaces to study local signaling in motor axon guidance. Our chamber system is designed to accommodate aggregate cultures, such as explants or embryoid bodies containing embryonic-stem-cell-derived neurons, both being more suitable for the study of axon guidance than dissociated cells. As a demonstration of this system, we investigate guidance of embryonic-stem-cell-derived motor neuron axons by *N*-cadherin, a well-known type I cadherin that mediates homophilic, calcium-dependent cell–cell interactions primarily involved in cell adhesion.[11] *N*-cadherin was recently shown to direct axon guidance and increase the rate of axonal extension.[12–16] These functions are mediated not only

[a]*Department of Biomedical Engineering, Columbia University, New York, NY, USA. E-mail: lk2141@columbia.edu*
[b]*Departments of Pathology, Neurology and Neuroscience, Center for Motor Neuron Biology and Disease, Columbia University Medical Center, New York, NY, USA*

† Electronic supplementary information (ESI) available: Time course of axon outgrowth under different conditions with/without targeted treatment of FGFR inhibitor. See DOI: 10.1039/b922143c

by classic cadherin–catenins interactions, but also by the activation of FGF receptors (FGFRs). Global interference of FGFR function inhibits *N*-cadherin induced axonal outgrowth in cerebellar granule neurons,[17,18] retinal ganglion cells,[19] and spinal cord explants.[20] Recent studies suggest that these interactions between FGFR and *N*-cadherin lead to activation of secondary messenger signaling cascades,[17,21,22] including the PLCγ/DAG lipase/CAM kinase/Ca^{2+} signaling pathway which in turn regulates axon growth.[19,23] Here, we utilize the combined compartmentalized chamber–micropatterned surface system to investigate how localization of FGFR and *N*-cadherin signaling within specific regions of the neuron influence axon guidance and growth; given the role of soluble, diffusing factors in the cross-talk between these pathways, it is possible that activation of these pathways in different parts of the cell combine globally to modulate axon growth. Alternatively, a requirement of localized co-activation for these pathways would provide new design principles for understanding neural development.

Results and discussion

Chamber design and fabrication

The technical goal of this study is to build a system that allows neurons to interact with and choose between multiple biomolecular signals while providing pharmacologically isolated access to axons and cell bodies. As illustrated in Fig. 1, our implementation consists of an elastomer (polydimethylsiloxane, PDMS) chamber with two open compartments, one for cell bodies and the other for axons, connected by a series of microscale channels that limit diffusion of chemicals between the compartments while allowing and directing axon growth between these structures. For this study, we chose an optimized set of microchannel dimensions of 500 μm in length, 10 μm in width, and 5 μm in height, with a center-to-center spacing of 25 μm, which supported good fluidic isolation between the two compartments while allowing robust axonal outgrowth. On the cell body side, we introduced into the microchannel barrier a 50 μm tall, 50 μm wide overhang (Fig. 1B) to hold the explants in close proximity to the barrier. The microchannels and overhang were cast from a multi-height master fabricated out of photoresist using conventional techniques. The resultant structure was cut to create compartments, and then assembled onto planar glass substrates (modified with protein patterns as described below) to produce the chamber device. The cell body and axon chambers were chemically well-isolated from each other, as illustrated in Fig. 2A. The axon chamber was loaded with 10 μM Cy5 fluorescent dye (M_W 792 Da) in cell culture media while the cell body side contained media alone. The fluorescence image was taken after incubating the chamber at 37 °C for 24 h. Minimal fluorescence was detected in the cell body compartment, demonstrating chamber isolation. Molecular transport simulations, assuming a typical diffusion coefficient of 1 $\mu m^2\ ms^{-1}$ for small molecular agents and the dimensions stated above, indicate that the concentration in the cell body compartment would reach 1.7% of axon compartment concentration after 24 h. This limited transport could be further compensated by maintaining the liquid level of the cell body compartment slightly higher than that of the axon compartment.[7] Simulations indicate that the modest rate of media flow (10 $\mu m\ s^{-1}$) created by increasing the liquid depth in the cell body side by 250 μm effectively offsets solute transport, resulting in 0.053% increase in the cell body compartment concentration over 24 h (Fig. 2B and C).

Proteins in the axon chamber are patterned onto the bottom surface prior to assembly. Specifically, we use an indirect affinity approach[9,10] to avoid drying and potential denaturation of the

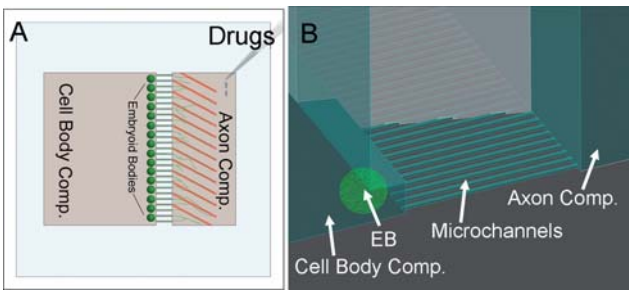

Fig. 1 System illustration. (A) Graphic representation of our chamber system for combining cell body/axon isolation and outgrowth selectivity. (B) The compartments are isolated by a microchannel barrier, containing a linear array of 10 μm wide, 5 μm high channels spaced 25 μm apart. An overhang in the region next to the barrier simplified loading of aggregate samples.

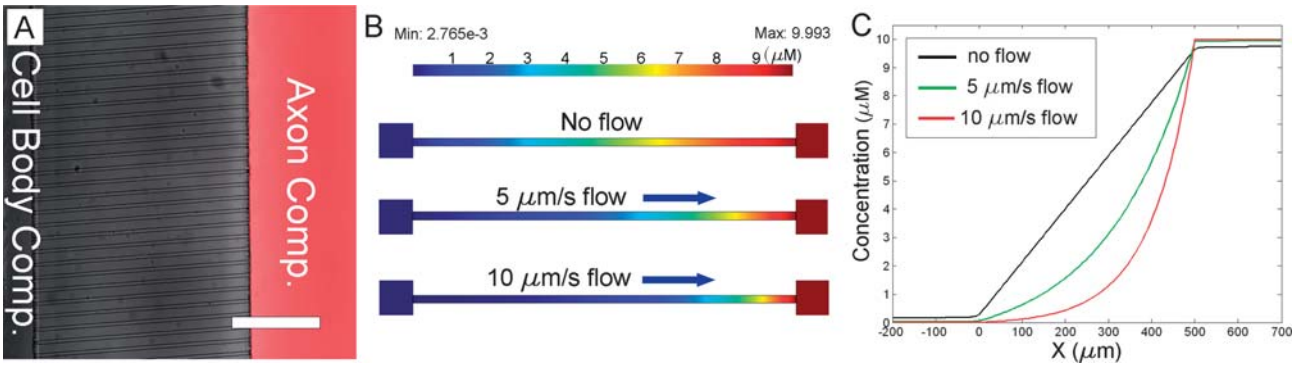

Fig. 2 Chemical isolation between compartments. (A) Fluidic isolation of Cy5 dye into the axonal compartment after 24 h incubation at 37 °C, scale bar: 200 μm. (B) Simulated distribution of a diffusing chemical under no-flow or pressure-driven flow conditions. Constant flows of 0, 5, and 10 $\mu m\ s^{-1}$. (C) Concentration profiles of diffusion under flow conditions, derived from the simulations shown in panel B.

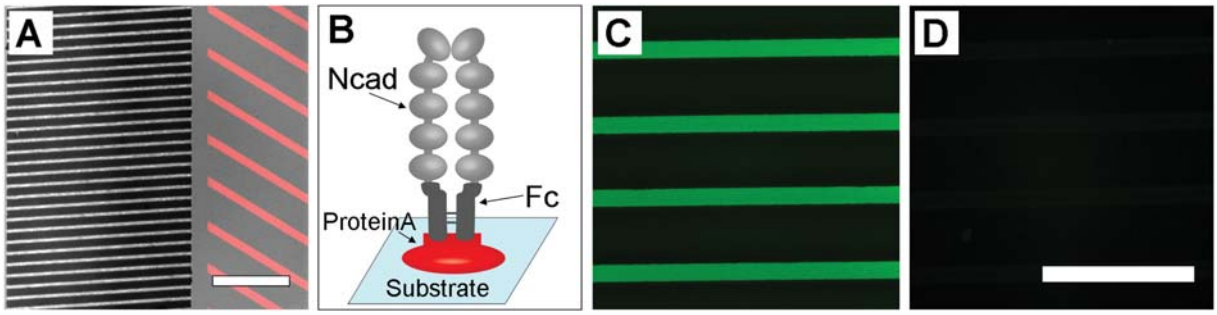

Fig. 3 Patterning of guidance proteins. (A) A combined internal reflection microscopy and fluorescence image showing alignment of microchannel walls (dark regions) with lines of protein A (red). (B) Fc-containing proteins are captured onto the patterned protein A. (C and D) Demonstration of indirect capture using Ncad–Fc (panel C) onto protein A. Fluorescently labeled fibronectin was not selectively captured onto these lines (panel D). Scale bar: 200 μm.

protein during chamber assembly. Microscale patterns of protein A are microcontact printed onto the coverslip, which is then aligned with the microchannel barrier using a custom-built aligner (Fig. 3A). A slight angle (typically 30°) between the stripes and microchannels is adopted to better detect axon guidance. After assembly, fusion proteins containing the active region of the target protein appended with an Fc domain were captured from solution by the patterned protein A (Fig. 3B). Fig. 3C illustrates the capture of Ncad–Fc, a fusion of the extracellular domain of *N*-cadherin with human Fc. The captured protein concentration was approximately 100 molecules per μm^2 as reported previously,[10] and this capture is specific, as incubation of a protein A-patterned surface (blocked with BSA) with fibronectin (which lacks an Fc domain) does not reveal similar patterning (Fig. 3D). This indirect capture approach is highly flexible, robust, and, as will be described later in this report, extensible to include multiple proteins.

Axon response in the microfabricated system

Fig. 4 illustrates the use of these chambers with motor neurons (MNs). HBG3 ES cells expressing a GFP transgene under the control of motor neuron specific promoter HB9 were differentiated as embryoid bodies (EBs) into spinal motor neurons.[24] Chambers were prepared by microcontact printing lines of protein A and backcoating sequentially with polyornithine and laminin, providing a permissive reference substrate; the activity of surface-captured Ncad–Fc or other target protein is evaluated in comparison to this surface. EBs were then loaded into the cell body compartment and manipulated into position under the overhang using a glass pipette. Fig. 4A illustrates the position of EBs against the barrier. Over the course of 48 h, axons extended from these EBs progress through the microchannels and interact with the target proteins. As illustrated in Fig. 4B, axons encountering lines of Ncad–Fc (25 μm width, spaced 75 μm apart) reoriented and followed these lines in contrast to the intervening regions of laminin alone (without *N*-cadherin) that did not elicit a turning response from motor axons. Axon guidance was *N*-cadherin specific, as axons on surfaces incubated with pre-immune rabbit IgG antibody were not similarly guided (Fig. 4C). To further demonstrate the specificity of *N*-cadherin guidance, we patterned chambers with a repulsive cue, an Fc-tagged version of EphrinB2 (Eph–Fc). Axons on these surfaces avoided the lines of Eph–Fc, growing instead preferentially along the intervening laminin regions (Fig. 4D). We thus demonstrated that the developed system can be utilized to study mechanisms underlying both attractive and repulsive axon guidance.

Local crosstalk between FGFR and *N*-cadherin signaling

The remainder of this report focuses on the main strength of our system, the ability to localize pharmacological interventions in

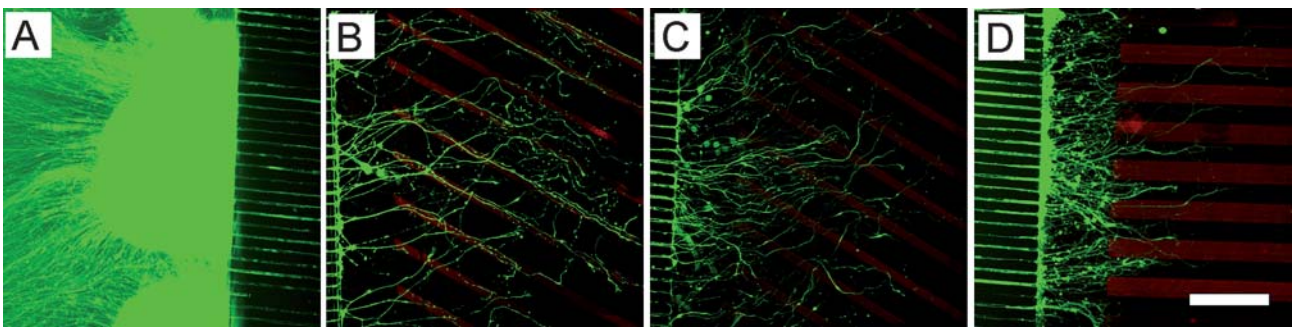

Fig. 4 Axon guidance in response to attractive and repulsive cues. (A) EBs containing motor neurons expressing GFP (green) and extending axons maintain close proximity to the microchannels. (B) Guidance of motor axons by Ncad–Fc captured onto the protein A lines (red). (C) No guidance was observed on patterned surfaces incubated with rabbit IgG. (D) EphrinB2–Fc, captured onto the protein A, repelled motor axons. Axon outgrowth was limited to the intervening regions of laminin. Scale bar: 200 μm.

order to identify the mechanisms of axon growth and guidance on micropatterned surfaces. We first quantified the guidance along *N*-cadherin stripes illustrated in Fig. 2B by measuring the angle formed between the microchannels and axons. Growth parallel to the microchannels and perpendicular to the barrier edge was chosen as a zero degree reference. Fig. 5A shows a histogram of the angle formed by individually identifiable axons on surfaces incubated with either Ncad–Fc or an inert antibody, collected from three separate experiments, measured 48 h after EB plating. For these studies, the protein A lines were patterned at an angle of 30°, and the increased population of axons extending along this direction illustrates guidance by Ncad–Fc. As a further comparison, Fig. 5B reports the fraction of axons extending along the protein A lines (within a ±10° window). The fraction of axons within this window is approximately four-fold higher on Ncad–Fc lines than on lines coated with the control antibody of rabbit IgG ($P < 0.001$ by ANOVA, $n = 3$, 179, and 184 axons drawn from three separate experiments).

N-Cadherin effects on axon outgrowth have been previously shown to depend upon FGFR signaling, but the localization of this crosstalk was not empirically determined. To examine whether the axon's guidance by Ncad–Fc is dependent on FGFR signaling, we measured the fraction of axons aligned along the Ncad–Fc lines (within the same window) in the presence of the FGFR inhibitor, PD173074. This inhibitor selectively blocks FGFR tyrosine kinase activity and autophosphorylation of FGFR.[25] When supplemented at 100 nM (a concentration previously demonstrated to disrupt FGFR signaling[20]) into either the axon or cell body compartment, PD173074 did not affect the preferential growth of axons along Ncad–Fc lines as illustrated by the last two columns of Fig. 5B ($P = 0.747$ by ANOVA, $n = 129$ and 168 axons drawn from three independent experiments, respectively). Thus, guidance selectivity of axons by *N*-cadherin is not dependent on local FGFR signaling.

We next examined the rate of axon outgrowth on Ncad–Fc as a function of FGFR inhibition. Outgrowth rate averaged over a 12 h period, starting at 36 h after seeding of EBs, is compared in Fig. 6, while representative time-lapse series images of axon outgrowth in the presence and absence of inhibitor are included in ESI I†. When added to the cell body compartment, PD173074 did not decrease the rate of axon outgrowth on Ncad–Fc, compared to that with no inhibitor ($P = 0.63$, $n = 86$ and 63 axons for uninhibited and cell body inhibited samples, drawn from three independent experiments). In contrast, FGFR inhibitor added to the axon compartment significantly reduced the rate of Ncad–Fc stimulated axon outgrowth by 40%, from 43.3 ± 15.9 μm h^{-1} to 24.1 ± 10.9 μm h^{-1}. ($P < 0.001$, mean ± s.d., $n = 94$ axons drawn from three experiments for axon-inhibition). Importantly, axon outgrowth rate on laminin (LN) coated stripes was not influenced by the presence of FGFR inhibitor in either compartment and stayed at a basal level in each condition. These results demonstrate that stimulation of axon outgrowth on *N*-cadherin depends on localized FGFR activation within the growth cones and axons.

These results are consistent with the model in which FGFR interacts locally with *N*-cadherin at the growth cone to stimulate axon outgrowth, but further indicate that biomolecules involved in intracellular signaling at distal sites of FGFR activation do not diffuse into the growth cone at levels sufficient to compensate for local loss of this stimulus. In particular, our results are

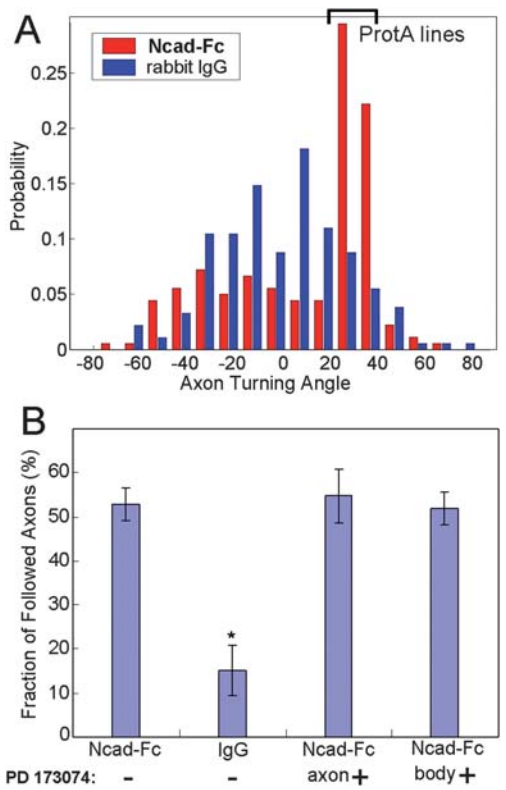

Fig. 5 Axon guidance on *N*-cadherin. (A) Histogram of axon extension angle by neurons on surfaces incubated with Ncad–Fc or rabbit IgG. (B) Fraction of axons extending along the protein A lines. Addition of FGFR inhibitor, PD173074, into either the axon or cell body compartment does not affect guidance on *N*-cadherin. Data are mean ± s.d. from three independent experiments representing a total of 179, 184, 129 and 168 axons for each of the four conditions, respectively. *$P < 0.001$ compared to Ncad–Fc in the absence of inhibitor, by ANOVA.

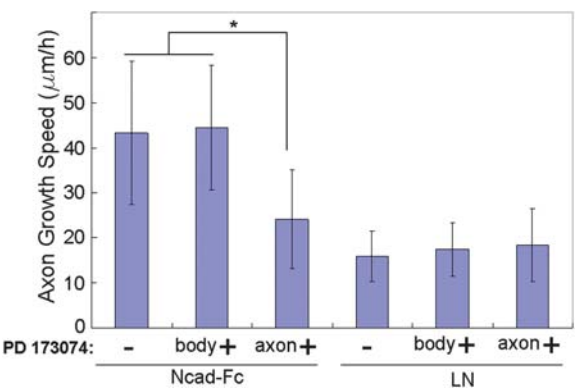

Fig. 6 Local crosstalk between FGFR and *N*-cadherin signaling. FGFR inhibitor impedes the ability of Ncad–Fc to stimulate axon outgrowth when targeted to the axonal compartment but not the body compartment. Similar effects of FGFR were not observed in axons growing on laminin region. Data are mean ± s.d. from three independent experiments, representing a total of 86, 63, 94, 51, 50, and 53 axons for each of the conditions (left-to-right). *$P < 0.001$ by ANOVA, comparisons only between axons on the same protein substrate.

consistent with recent studies implicating the PLCγ/DAG lipase/CAM kinase/Ca^{2+} signaling pathway[19,23] in coordinating FGFR/*N*-cadherin crosstalk; with the increasing recognition even highly diffusible second messengers such as Ca^{2+} can be compartmentalized, in this case to the cell body *vs.* axon, our results suggest a functional impact of this localized signaling.

Conclusion

It is increasingly recognized that intracellular signaling must be considered on a localized basis over a wide range of spatial scales, ranging from nanometres to several centimetres. In this report, microfabricated Campenot chambers are combined with multi-component, micropatterned surfaces to demonstrate that different aspects of axon guidance by *N*-cadherin occur through different signaling pathways. Local crosstalk between *N*-cadherin and FGFR within the axon of motor neurons is essential for stimulating axon outgrowth, but not guidance along *N*-cadherin. Further development of this system will provide finer spatial and temporal resolution for the manipulation of cell signaling, allowing entirely new levels of investigation into how cells interpret the complex extracellular environment during development and repair, including the roles of local protein synthesis and second messenger activation.

Finally, we note that the combined chamber–patterned surface platform developed here will be of use in many studies of cellular signaling, specifically those that focus on cells of extended morphology. This includes neuron and neural cells of multiple systems, including not only visual and auditory networks, but also epithelial and endothelial systems. In all cases, understanding how the local interaction/crosstalk of matrix-bound and soluble cues, along with cell morphology, drive tissue function and repair will be accelerated by systems such as the one we present here. More complex studies of cell response to multiple signals or to signal gradients[10,26] will also be made possible by this platform.

Experimental

Device fabrication

Microfluidic chambers are fabricated using soft lithography technique[27] using a two-layer fabrication process.[6] The device consists of two open compartments bridged by multiple microchannels (5 μm depth, 10 μm width, and 500 μm length). A silicon wafer is spin-coated with a first layer of photoresist SU 8-2005 (5 μm), and exposed through a mask forming the layout of the microchannels. After development, a second layer of SU8-2050 (50 μm) is spin-coated and exposed through a mask containing patterns of both chambers, resulting in a master with positive relief patterns of the microfluidic device. A pre-polymer mixture of Sylgard 184 (Dow Corning) is cast against the master and cured to obtain a negative replica-molded piece. Two culture compartments are then cut into the elastomer, presenting the final chamber structure. The chambers are plasma treated for 2 min before assembling with a patterned coverslip to promote fluidic sealing of the final device.

Protein patterning and substrate preparation

Before patterning proteins, coverslips (25 mm, Fisher Scientific) were cleaned in Linbro 7× detergent (ICN, mixed 1 : 4 with deionized water) at 80 °C for 45 min, rinsed extensively with deionized water, and baked at 450 °C for 6 h. Protein A is patterned at a specific location of each coverslip through microcontact printing. Briefly, PDMS stamps containing designed geometries were coated with 20 μg ml^{-1} protein A in PBS for 1 h. For visualization purpose, 1/6 of the protein A was prelabeled with Cy5 (GE Healthcare). The stamp was washed with DI water and dried by blowing nitrogen gas and placed in contact with the substrate for 10 s. The coverslip was further plasma treated for 2 min with the stamped region covered by a piece of plain PDMS.

The prepared chamber piece was assembled with the coverslips under our 6-axis aligner, to ensure that the exit of the microchannels is close to the protein A patterns. The entire inner surface of the chamber was blocked with 4% BSA for 2 h. The axon compartments were then exposed to either Ncad–Fc (5 μg ml^{-1}, R&D Systems) or Ephrin–Fc (10 μg ml^{-1}) in PBS + 4% bovine serum albumin (BSA, Sigma) for 45 min at room temperature, and finally rinsed with PBS. And then, both compartments were sequentially incubated with polyornithine (Sigma) overnight (10 μg ml^{-1} for cell body chamber, 2 μg ml^{-1} for axon chamber) and laminin (10 μg ml^{-1}, Invitrogen) for 1 h before loading EBs.

Cell culture

All culture reagents are from Invitrogen, unless otherwise stated. Embryoid body preparations of rostral cervical motor neurons (MNs) were produced by addition of retinoic acid and hedgehog agonist to embryonic-stem-cell lines as previously described.[24,28] Briefly, HB9::GFP transgenic mouse-derived (HBG3) ES cells were grown on mouse embryonic fibroblasts in ES cell medium. ES cell colonies were dissociated after 2 days and cultured in DFK5 media. Media were replaced at 2 days and supplemented with all *trans* retinoic acid (1 μM, Sigma) and hedgehog agonist SAG (500 nM, Calbiochem). Medium was replaced on day 5 of differentiation and embryoid bodies (EBs) containing MNs were harvested on day 6–7 for use in the axon guidance studies. Once placed in the compartmentalized chamber system, EBs were cultured in Neurobasal medium containing B27 supplements, 2 μM L-glutamine, and antibiotics.

Imaging and quantification

The cultures were observed by fluorescent and bright-field microscopy using a 10× objective on an inverted Olympus IX71 microscope. During imaging, the temperature and CO_2 level were maintained at 37 °C and 5% respectively using a live-cell imaging chamber (Pathology Devices, MD). To quantify the axons' growth speed, images were taken at 12 h interval to identify the extended length of each axon during that period, and to derive the averaged hourly growth rate.

Molecular transport simulation

Simulation of diffusive transport in the channels was done by finite element methods, using the COMSOL software package (COMSOL Multiphysics v3.2, Burlington,MA). The simulations presented here use the convection–diffusion model and assume a diffusion coefficient of 1 $\mu m^2\ ms^{-1}$ and media viscosity at 37 °C

of $\mu = 6.92 \times 10^{-4}$ Pa s. The initial concentration of chemical in the axon compartment was 10 μM, and set to zero in the other compartment. For calculations of flow *versus* pressure head difference, the resistance of the rectangle microscale channels, which measured 500 μm in length (L), 10 μm in width (w), and 5 μm in height (h), was estimated as $R \approx 12\,\mu L/(h^3 w(1 - 0.63h/w))$.[29]

Acknowledgements

This work was supported by Columbia University through the Research Initiatives in Science and Engineering program. The CEPSR clean room at Columbia University is also acknowledged for assistance in microfabrication.

References

1 B. J. Dickson, *Science*, 2002, **298**, 1959–1964.
2 R. B. Campenot, *Proc. Natl. Acad. Sci. U. S. A.*, 1977, **74**, 4516–4519.
3 B. Campenot, K. Lund and D. L. Senger, *J. Cell Biol.*, 1996, **135**, 701–709.
4 B. L. MacInnis and R. B. Campenot, *Science*, 2002, **295**, 1536–1539.
5 U. Hengst, A. Deglincerti, H. J. Kim, N. L. Jeon and S. R. Jaffrey, *Nat. Cell Biol.*, 2009, **11**, 1024–1030.
6 J. W. Park, B. Vahidi, A. M. Taylor, S. W. Rhee and N. L. Jeon, *Nat. Protoc.*, 2006, **1**, 2128–2136.
7 A. M. Taylor, M. Blurton-Jones, S. W. Rhee, D. H. Cribbs, C. W. Cotman and N. L. Jeon, *Nat. Methods*, 2005, **2**, 599–605.
8 A. M. Taylor, S. W. Rhee, C. H. Tu, D. H. Cribbs, C. W. Cotman and N. L. Jeon, *Langmuir*, 2002, **19**, 1551–1556.
9 A. A. Oliva, Jr., C. D. James, C. E. Kingman, H. G. Craighead and G. A. Banker, *Neurochem. Res.*, 2003, **28**, 1639–1648.
10 P. Shi, K. Shen and L. C. Kam, *Dev. Neurobiol.*, 2007, **67**, 1765–1776.
11 U. Tepass, K. Truong, D. Godt, M. Ikura and M. Peifer, *Nat. Rev. Mol. Cell Biol.*, 2000, **1**, 91–100.
12 M. Kadowaki, S. Nakamura, O. Machon, S. Krauss, G. L. Radice and M. Takeichi, *Dev. Biol.*, 2007, **304**, 22–33.
13 R. Riehl, K. Johnson, R. Bradley, G. B. Grunwald, E. Cornel, A. Lilienbaum and C. E. Holt, *Neuron*, 1996, **17**, 837–848.
14 X. Yu and R. C. Malenka, *Nat. Neurosci.*, 2003, **6**, 1169–1177.
15 D. L. Benson and H. Tanaka, *J. Neurosci.*, 1998, **18**, 6892–6904.
16 K. Okamura, H. Tanaka, Y. Yagita, Y. Saeki, A. Taguchi, Y. Hiraoka, L. H. Zeng, D. R. Colman and N. Miki, *J. Cell Biol.*, 2004, **167**, 961–972.
17 E. J. Williams, G. Williams, F. V. Howell, S. D. Skaper, F. S. Walsh and P. Doherty, *J. Biol. Chem.*, 2001, **276**, 43879–43886.
18 J. L. Saffell, E. J. Williams, I. J. Mason, F. S. Walsh and P. Doherty, *Neuron*, 1997, **18**, 231–242.
19 B. Lom, V. Hopker, S. McFarlane, J. L. Bixby and C. E. Holt, *J. Neurobiol.*, 1998, **37**, 633–641.
20 C. Boscher and R. M. Mege, *Cell. Signalling*, 2008, **20**, 1061–1072.
21 E. Sanchez-Heras, F. V. Howell, G. Williams and P. Doherty, *J. Biol. Chem.*, 2006, **281**, 35208–35216.
22 K. Suyama, I. Shapiro, M. Guttman and R. B. Hazan, *Cancer Cell*, 2002, **2**, 301–314.
23 E. J. Williams, F. S. Walsh and P. Doherty, *J. Cell Biol.*, 2003, **160**, 481–486.
24 H. Wichterle, I. Lieberam, J. A. Porter and T. M. Jessell, *Cell*, 2002, **110**, 385–397.
25 M. Mohammadi, S. Froum, J. M. Hamby, M. C. Schroeder, R. L. Panek, G. H. Lu, A. V. Eliseenkova, D. Green, J. Schlessinger and S. R. Hubbard, *EMBO J.*, 1998, **17**, 5896–5904.
26 A. C. von Philipsborn, S. Lang, J. Loeschinger, A. Bernard, C. David, D. Lehnert, F. Bonhoeffer and M. Bastmeyer, *Development (Cambridge, UK)*, 2006, **133**, 2487–2495.
27 G. M. Whitesides, *Nature*, 2006, **442**, 368–373.
28 H. Wichterle and M. Peljto, *Curr. Protoc. Stem Cell Biol.*, 2008, **1**, 1H.1.1–1H.1.9.
29 H. A. Stone, A. D. Stroock and A. Ajdari, *Annu. Rev. Fluid Mech.*, 2004, **36**, 381–411.

